Eur. Phys. J. C (2014) 74:2927
DOI 10.1140/epjc/s10052-014-2927-y

THE EUROPEAN PHYSICAL JOURNAL C

Regular Article - Theoretical Physics

$B \to K^*\mu^+\mu^-$ optimised observables in the MSSM

Farvah Mahmoudi[1,2,a], **Siavash Neshatpour**[1,3,b], **Javier Virto**[4,c]

[1] Clermont Université, Université Blaise Pascal, CNRS/IN2P3, LPC, BP 10448, 63000 Clermont-Ferrand, France
[2] CERN Theory Division, Physics Department, 1211 Geneva 23, Switzerland
[3] Department of Physics, Isfahan University of Technology, 84156-83111 Isfahan, Iran
[4] Theoretische Physik 1, Naturwissenschaftlich-Technische Fakultät, Universität Siegen, 57068 Siegen, Germany

Received: 14 January 2014 / Accepted: 29 May 2014 / Published online: 24 June 2014

Abstract We provide a detailed analysis of the impact of the newly measured optimised observables in the $B \to K^*\mu^+\mu^-$ decay by the LHCb experiment. The analysis is performed in the MSSM, both in the context of the usual constrained scenarios and in the context of a more general set-up where the SUSY partner masses are independent. We show that the global agreement of the MSSM solutions with the data is still very good. Nevertheless, especially in the constrained scenarios, the limits from $B \to K^*\mu^+\mu^-$ are now very strong and are at the same level as the well-known $b \to s\gamma$ constraints. We describe the implications of the $B \to K^*\mu^+\mu^-$ measurements both on the Wilson coefficients and on the SUSY parameters.

1 Introduction

Rare $b \to s$ transitions provide a powerful probe of the flavour sector of the Standard Model (SM). The effective Hamiltonian formulation of these processes allows for a convenient low-energy description in terms of short distance Wilson coefficients $\mathcal{C}_i$. Deviations from the SM predictions can then be consistently parametrised in terms of New Physics (NP) contributions to the Wilson coefficients ($\delta\mathcal{C}_i \equiv \mathcal{C}_i - \mathcal{C}_i^{\rm SM}$). In addition, model predictions for the coefficients $\delta\mathcal{C}_i$ can be computed by matching the model to the effective theory at the electroweak scale; thus these coefficients provide a link between the high-energy model and the low-energy phenomenology. In the case of $b \to s$ transitions, the relevant $d = 6$ Hamiltonian is given by

$$\mathcal{H}_{\rm eff} = \mathcal{H}_{\rm eff}^{\rm sl} + \mathcal{H}_{\rm eff}^{\rm had}, \tag{1.1}$$

where the semileptonic part $\mathcal{H}_{\rm eff}^{\rm sl}$ is composed of radiative and dileptonic operators $[\bar{s}\Gamma^{\mu\nu}b]F_{\mu\nu}$ and $[\bar{s}\Gamma b][\bar{\ell}\Gamma'\ell]$, and the hadronic part $\mathcal{H}_{\rm eff}^{\rm had}$ contains chromomagnetic $[\bar{s}\Gamma^{\mu\nu}b]G_{\mu\nu}$ and 4-quark operators $[\bar{s}\Gamma b][\bar{q}_1\Gamma' q_2]$.

Recently, a significant amount of work has been devoted to the study of $b \to s\ell\ell$ processes [1–11], where experimental progress has been outstanding (see *e.g.* Refs. [12–16]). These processes are the most sensitive to $\mathcal{H}_{\rm eff}^{\rm sl}$ and, together with $b \to s\gamma$ processes, pose strong conditions on the corresponding Wilson coefficients. More specifically, $\mathcal{H}_{\rm eff}^{\rm sl}$ is given by

$$\mathcal{H}_{\rm eff}^{\rm sl} = -\frac{4G_F}{\sqrt{2}} V_{tb}V_{ts}^* \left[\sum_{i=7,9,10} \left(\mathcal{C}_i\mathcal{O}_i + \mathcal{C}_i'\mathcal{O}_i'\right) + \sum_{i=1,2} \left(\mathcal{C}_{Q_i} Q_i + \mathcal{C}'_{Q_i} Q'_i\right) \right]. \tag{1.2}$$

The various operators in $\mathcal{H}_{\rm eff}^{\rm sl}$ as well as the chromomagnetic operator $\mathcal{O}_8$ are defined as

$$\begin{aligned}
\mathcal{O}_7^{(\prime)} &= \frac{e}{(4\pi)^2} m_b [\bar{s}\sigma^{\mu\nu} P_{R(L)} b] F_{\mu\nu}, \\
\mathcal{O}_8^{(\prime)} &= \frac{g}{(4\pi)^2} m_b [\bar{s}\sigma^{\mu\nu} T^a P_{R(L)} b] G^a_{\mu\nu}, \\
\mathcal{O}_9^{(\prime)} &= \frac{e^2}{(4\pi)^2} [\bar{s}\gamma^\mu P_{L(R)} b][\bar{\ell}\gamma_\mu \ell], \\
\mathcal{O}_{10}^{(\prime)} &= \frac{e^2}{(4\pi)^2} [\bar{s}\gamma^\mu P_{L(R)} b][\bar{\ell}\gamma_\mu\gamma_5 \ell], \\
Q_1^{(\prime)} &= \frac{e^2}{(4\pi)^2} [\bar{s} P_{R(L)} b][\bar{\ell}\,\ell], \\
Q_2^{(\prime)} &= \frac{e^2}{(4\pi)^2} [\bar{s} P_{R(L)} b][\bar{\ell}\gamma_5 \ell],
\end{aligned} \tag{1.3}$$

where $Q_{1,2}$ are the scalar and pseudo-scalar operators, related to the usual $\mathcal{O}_{S,P}^{(\prime)}$ by the running b-quark mass: $\mathcal{O}_{S,P}^{(\prime)} = \hat{m}_b\, Q_{1,2}^{(\prime)}$ (see *e.g.* Ref. [17]). We have neglected the tensor

[a] e-mail: mahmoudi@in2p3.fr
[b] e-mail: neshatpour@clermont.in2p3.fr
[c] e-mail: virto@physik.uni-siegen.de

operators as they are highly suppressed both in the SM and in the Minimal Supersymmetric Standard Model (MSSM). The corresponding Wilson coefficients are well known in the SM [18–24], where $\mathcal{C}_7^{\rm SM} = -0.297$, $\mathcal{C}_8^{\rm SM} = -0.161$, $\mathcal{C}_9^{\rm SM} = 4.22$ and $\mathcal{C}_{10}^{\rm SM} = -4.15$ at the scale of the b-quark pole mass ($\mu = m_b^{\rm pole}$), while their primed counterparts as well as the scalar and pseudo-scalar Wilson coefficients vanish to a good approximation. Global fits to all available $b \to s\gamma$ and $b \to s\mu^+\mu^-$ data constrain significantly the allowed values for the NP contributions $\delta\mathcal{C}_i$ [25–28], specially when the latest $B \to K^*\mu^+\mu^-$ data is included [1–4].

It is precisely the decay $B \to K^*(\to K\pi)\mu^+\mu^-$ that has attracted most of the attention recently. Its angular distribution [29,30] (see also *e.g.* [17,31,32]) provides a plethora of observables sensitive to different helicity structures in the decay amplitude. However, theoretical predictions for the most obvious observables inherit large uncertainties from not-so-well-known hadronic form factors. This has led to the construction of a number of *optimised* observables as appropriate ratios of angular coefficients where most of the dependence on the form factors cancels, while having high sensitivity to NP effects [28,33–37]. A complete minimal set of such observables is given by the $\{P_i^{(\prime)}\}$ ensemble [28,35]. Rigorous SM predictions for these and other $B \to K^*\mu^+\mu^-$ observables can be found in Ref. [38] and are also implemented within `SuperIso` [39,40].

While all previous experimental results from rare $|\Delta B| = |\Delta S| = 1$ processes were pointing to SM like values for the Wilson coefficients, the bounds on dileptonic operators were relatively mild, still allowing $|\delta\mathcal{C}_{9,10}{}^{(\prime)}/\mathcal{C}_{9,10}^{\rm SM\,(\prime)}| \sim \mathcal{O}(1)$ [28]. First measurements of the full angular distribution by the LHCb collaboration [12,13] have changed the situation, presenting a tension in several binned observables, such as P_2 and P_5'.

In Ref. [1], the first model-independent global fit for the Wilson coefficients using the recent LHCb results on $B \to K^*\mu^+\mu^-$ combined with other existing $b \to s$ data was performed, hinting to a rather large negative NP contribution $\delta\mathcal{C}_9 \sim -1.2$. This was followed by a global fit in Ref. [2], indicating a value close to $\delta\mathcal{C}_9 \sim -0.9$ (in agreement with Ref. [1]), and a global Bayesian fit in Ref. [3] with a best fit value for $\delta\mathcal{C}_9$ of either -1.3 or -0.3 depending on the set of observables used. An independent check has been given in Ref. [5]: a fit to $B \to K^*\mu^+\mu^-$ and $B_s \to \phi\mu^+\mu^-$ observables at low hadronic recoil only, based on the recent unquenched lattice results for the relevant form factors [6], leads to a similar value for $\delta\mathcal{C}_9 \sim -1$. In Ref. [4] it was argued that a consistent New Physics explanation of the $\bar{B} \to \bar{K}^*\mu^+\mu^-$ results in the context of minimal flavour violation is possible.

The model-independent global fits require $\mathcal{C}_7$ and $\mathcal{C}_{10}$ to be close to their SM values (in order to satisfy the strong $B \to X_s\gamma$ and $B_s \to \mu^+\mu^-$ constraints). This has promoted NP scenarios where $\delta\mathcal{C}_7^{(\prime)}$ and $\delta\mathcal{C}_{10}^{(\prime)}$ are negligible while $\delta\mathcal{C}_9 \sim -1$, as is the case with models with a Z' gauge boson coupling to left- and right-handed leptons with equal strength [1,7,41] (arising for example in the 331 models [9,42]) or scenarios with effective four-quark scalar interactions [10]. A rather complete account of $Z^{(\prime)}$ FCNCs in relation to the recent $b \to s\mu\mu$ data has been given in [8]. It has also been argued that within SUSY models or in models with partial compositeness, such large values for $\delta\mathcal{C}_9$ can hardly be obtained [2]. In the analysis of Ref. [4] a different statistical method based on the absolute χ^2 (rather than $\Delta\chi^2$, which probes the area around a unique best fit point) revealed that larger sets of solutions can be obtained consistent with the latest $\bar{B} \to \bar{K}^*\mu^+\mu^-$ in the context of minimal flavour violation. In particular, while the deviation observed in P_5' favours values of $\delta\mathcal{C}_9 \sim -1$, it is still possible to have a *global* agreement with $b \to s$ data at the 1σ level with also SM like values of $\mathcal{C}_9$, as well as a set of solutions with flipped sign SM Wilson coefficients which has only a slightly larger χ^2, although this scenario is considerably more aggressive in terms of New Physics.

It is worth recalling that several studies (see for example [3,4]) show that at least part of the observed tension can also be explained by re-evaluating the theoretical uncertainties of the SM predictions, specially the ones due to power corrections. In particular in [4] good agreement with the SM was found assuming subleading power corrections of about 15 % at large hadronic recoil. But this is still an open issue.

On the other hand, assuming that the observed deviations are due to New Physics effects, the $\bar{B} \to \bar{K}^*\mu^+\mu^-$ decay has already been used to constrain the MSSM parameters (see e.g. [43,44]). In this work we study the implications of recent LHCb results for the $\bar{B} \to \bar{K}^*\mu^+\mu^-$ decay (combined with existing experimental results for other $b \to s$ transitions) on the MSSM. While we know that $\delta\mathcal{C}_9 \sim -1$ cannot be reached in the MSSM, the question of whether MSSM can nevertheless provide solutions which could be globally in agreement with the full set of $\bar{B} \to \bar{K}^*\mu^+\mu^-$ data seems an obvious and important one. Hence, in this study, we search for MSSM solutions which are consistent with a global fit to $b \to s$ data, based on a similar statistical approach as in Ref. [4].

Our numerical analysis is performed with `SOFTSUSY` [45] and `SuperIso` [39,40] and we study two classes of scenarios within the MSSM: the constrained MSSM models CMSSM and the Non Universal Higgs Mass (NUHM) model and a more general set-up known as phenomenological MSSM (pMSSM) which enables access to regions of the MSSM parameter space otherwise inaccessible with the aforementioned constrained scenarios. To investigate the viability of the MSSM scenarios considering recent experimental results on $\bar{B} \to \bar{K}^*\mu^+\mu^-$ observables, we perform a model-dependent analysis on the Wilson coefficients using

the other relevant $b \to s$ modes as well. Using this global analysis, constraints are obtained for several SUSY parameters within each scenario.

This paper is organised as follows: in Sect. 2 we provide the SM predictions and errors for $\bar{B} \to \bar{K}^* \mu^+ \mu^-$ observables as well as the other $b \to s$ processes considered in this work. In Sect. 3 we present the parameter ranges within which the MSSM scenarios that we have considered are investigated. Our statistical treatment is described in Sect. 4, and Sect. 5 contains our results on the global analysis. Conclusions are given in Sect. 6.

2 Optimised observables

Angular observables in $\bar{B} \to \bar{K}^*(\to K\pi)\mu^+\mu^-$ arise from the differential decay rate:

$$\begin{aligned}
&\frac{\mathrm{d}^4\Gamma(\bar{B}_d)}{\mathrm{d}q^2\,\mathrm{d}\cos\theta_K\,\mathrm{d}\cos\theta_l\,\mathrm{d}\phi} \\
&= \frac{9}{32\pi}\Big[J_{1s}\sin^2\theta_K + J_{1c}\cos^2\theta_K \\
&\quad + (J_{2s}\sin^2\theta_K + J_{2c}\cos^2\theta_K)\cos 2\theta_l \\
&\quad + J_3 \sin^2\theta_K \sin^2\theta_l \cos 2\phi + J_4 \sin 2\theta_K \sin 2\theta_l \cos\phi \\
&\quad + J_5 \sin 2\theta_K \sin\theta_l \cos\phi \\
&\quad + (J_{6s}\sin^2\theta_K + J_{6c}\cos^2\theta_K)\cos\theta_l \\
&\quad + J_7 \sin 2\theta_K \sin\theta_l \sin\phi + J_8 \sin 2\theta_K \sin 2\theta_l \sin\phi \\
&\quad + J_9 \sin^2\theta_K \sin^2\theta_l \sin 2\phi \Big],
\end{aligned} \tag{2.1}$$

where notation and conventions follow Refs. [17,35,36]. Here we focus on CP-averaged quantities, for which the angular distribution $\mathrm{d}\bar{\Gamma}$ of the CP-conjugated process $B \to K^*\mu^+\mu^-$ must also be considered. This is obtained from Eq. (2.1) by replacing $J_{1,2,3,4,7} \to \bar{J}_{1,2,3,4,7}$ and $J_{5,6,8,9} \to -\bar{J}_{5,6,8,9}$, where $\bar{J}$ is equal to J with all weak phases conjugated (see e.g. Ref. [29]).

The basic observables are the functions $J_i(q^2)$ integrated in q^2-bins (q^2 is the squared invariant mass of the muon pair). From these a number of *optimised* observables can be constructed, where some hadronic uncertainties are minimised by taking appropriate ratios. A set of such optimised observables have been measured recently by the LHCb collaboration [12,13], these are defined as [28,35,38]:

$$\begin{aligned}
\langle P_1\rangle_{\mathrm{bin}} &= \frac{1}{2}\frac{\int_{\mathrm{bin}} \mathrm{d}q^2 [J_3 + \bar{J}_3]}{\int_{\mathrm{bin}} \mathrm{d}q^2 [J_{2s} + \bar{J}_{2s}]}, \\
\langle P_2\rangle_{\mathrm{bin}} &= \frac{1}{8}\frac{\int_{\mathrm{bin}} \mathrm{d}q^2 [J_{6s} + \bar{J}_{6s}]}{\int_{\mathrm{bin}} \mathrm{d}q^2 [J_{2s} + \bar{J}_{2s}]},
\end{aligned}$$

$$\begin{aligned}
\langle P'_4\rangle_{\mathrm{bin}} &= \frac{1}{\mathcal{N}'_{\mathrm{bin}}}\int_{\mathrm{bin}} \mathrm{d}q^2 [J_4 + \bar{J}_4], \\
\langle P'_5\rangle_{\mathrm{bin}} &= \frac{1}{2\mathcal{N}'_{\mathrm{bin}}}\int_{\mathrm{bin}} \mathrm{d}q^2 [J_5 + \bar{J}_5], \\
\langle P'_6\rangle_{\mathrm{bin}} &= \frac{-1}{2\mathcal{N}'_{\mathrm{bin}}}\int_{\mathrm{bin}} \mathrm{d}q^2 [J_7 + \bar{J}_7], \\
\langle P'_8\rangle_{\mathrm{bin}} &= \frac{-1}{\mathcal{N}'_{\mathrm{bin}}}\int_{\mathrm{bin}} \mathrm{d}q^2 [J_8 + \bar{J}_8],
\end{aligned} \tag{2.2}$$

where the normalisation $\mathcal{N}'_{\mathrm{bin}}$ is given by

$$\mathcal{N}'_{\mathrm{bin}} = \sqrt{-\int_{\mathrm{bin}} \mathrm{d}q^2 [J_{2s} + \bar{J}_{2s}] \int_{\mathrm{bin}} \mathrm{d}q^2 [J_{2c} + \bar{J}_{2c}]}. \tag{2.3}$$

In addition, several non-optimised observables can be introduced in the analysis which are theoretically independent from the previous ones. In this paper we will consider the branching ratio and the longitudinal polarisation fraction:

$$\begin{aligned}
\langle \mathrm{dBR}/\mathrm{d}q^2\rangle_{\mathrm{bin}} &= \tau_B \frac{\langle \mathrm{d}\Gamma/\mathrm{d}q^2\rangle_{\mathrm{bin}} + \langle \mathrm{d}\bar{\Gamma}/\mathrm{d}q^2\rangle_{\mathrm{bin}}}{2}, \\
\langle F_L\rangle_{\mathrm{bin}} &= -\frac{\int_{\mathrm{bin}} \mathrm{d}q^2 [J_{2c} + \bar{J}_{2c}]}{\langle \mathrm{d}\Gamma/\mathrm{d}q^2\rangle + \langle \mathrm{d}\bar{\Gamma}/\mathrm{d}q^2\rangle},
\end{aligned} \tag{2.4}$$

where

$$\langle \mathrm{d}\Gamma/\mathrm{d}q^2\rangle_{\mathrm{bin}} = \frac{1}{4}\int_{\mathrm{bin}} \mathrm{d}q^2 [3J_{1c} + 6J_{1s} - J_{2c} - 2J_{2s}] \tag{2.5}$$

and analogously for $\bar{\Gamma}$. We do not consider the forward–backward asymmetry, which is significantly correlated to the observable P_2 [4]. The set of SM predictions and experimental measurements for all these observables are summarised in Table 1.

For the computation of these $B \to K^*\mu^+\mu^-$ observables in terms of the Wilson coefficients we follow Ref. [38]. At large recoil (low q^2) the theoretical tools are those of QCDF/SCET as described in Refs. [46,47]. In this kinematical region several form-factor relations [48,49] allow one to build the various optimised observables [28,35,38]. At low recoil (large q^2) the computation relies on an OPE for the relevant non-local hadronic matrix element, either in full QCD [50] or within the HQET [51]. Form-factor relations arise in HQET, allowing to construct optimised observables in this kinematic region [36–38], but the observables in Eq. (2.2) are not optimised at low recoil. The full form factors needed as an input are taken from the large-recoil LCSR computation in Ref. [52]. These are extrapolated to the low-recoil region following the procedure detailed in Ref. [38], and they are consistent with lattice QCD results in this region [6,53], as well as with HQET form-factor relations [38,51], for which a 20 % error from $1/m_b$ power corrections is included. Concerning power corrections to the hadronic contribution at low recoil, a 10 % error is added to each amplitude in an uncorrelated

Table 1 The most recent experimental values and SM predictions for the observables used in this study. Experimental error bars are symmetrised by taking the largest sided uncertainty to both sides. Pulls are therefore slightly different with respect to Ref. [1]. The several sources of uncertainty are added in quadrature.

Observable	Experiment	SM prediction	Pull
$10^4 \mathrm{BR}(B \to X_s\gamma)$	3.43 ± 0.22	3.09 ± 0.24	$+1.0$
$10^2 \Delta_0(B \to K^*\gamma)$	5.2 ± 2.6	7.9 ± 3.9	-0.6
$10^9 \mathrm{BR}(B_s \to \mu^+\mu^-)$	2.9 ± 0.7	3.49 ± 0.38	-0.7
$10^6 \mathrm{BR}(B \to X_s\mu^+\mu^-)_{q^2\in[1,6]\mathrm{GeV}^2}$	1.60 ± 0.68	1.73 ± 0.16	-0.2
$10^6 \mathrm{BR}(B \to X_s\mu^+\mu^-)_{q^2>14.4\mathrm{GeV}^2}$	0.42 ± 0.14	0.22 ± 0.04	$+1.4$
$10^7 \langle \mathrm{dBR}/\mathrm{d}q^2(B \to K^*\mu^+\mu^-)\rangle_{q^2\in[0.1,2]\mathrm{GeV}^2}$	0.60 ± 0.10	0.70 ± 0.81	-0.1
$\langle F_L(B \to K^*\mu^+\mu^-)\rangle_{q^2\in[0.1,2]\mathrm{GeV}^2}$	0.37 ± 0.11	0.32 ± 0.20	$+0.2$
$\langle P_1(B \to K^*\mu^+\mu^-)\rangle_{q^2\in[0.1,2]\mathrm{GeV}^2}$	-0.19 ± 0.40	-0.01 ± 0.04	-0.4
$\langle P_2(B \to K^*\mu^+\mu^-)\rangle_{q^2\in[0.1,2]\mathrm{GeV}^2}$	0.03 ± 0.15	0.17 ± 0.02	-0.9
$\langle P_4'(B \to K^*\mu^+\mu^-)\rangle_{q^2\in[0.1,2]\mathrm{GeV}^2}$	0.00 ± 0.52	-0.37 ± 0.03	$+0.7$
$\langle P_5'(B \to K^*\mu^+\mu^-)\rangle_{q^2\in[0.1,2]\mathrm{GeV}^2}$	0.45 ± 0.24	0.52 ± 0.04	-0.3
$\langle P_6'(B \to K^*\mu^+\mu^-)\rangle_{q^2\in[0.1,2]\mathrm{GeV}^2}$	0.24 ± 0.23	-0.05 ± 0.04	$+1.3$
$\langle P_8'(B \to K^*\mu^+\mu^-)\rangle_{q^2\in[0.1,2]\mathrm{GeV}^2}$	-0.12 ± 0.56	0.02 ± 0.04	-0.2
$10^7 \langle \mathrm{dBR}/\mathrm{d}q^2(B \to K^*\mu^+\mu^-)\rangle_{q^2\in[2,4.3]\mathrm{GeV}^2}$	0.30 ± 0.05	0.35 ± 0.29	-0.2
$\langle F_L(B \to K^*\mu^+\mu^-)\rangle_{q^2\in[2,4.3]\mathrm{GeV}^2}$	0.74 ± 0.10	0.76 ± 0.20	-0.1
$\langle P_1(B \to K^*\mu^+\mu^-)\rangle_{q^2\in[2,4.3]\mathrm{GeV}^2}$	-0.29 ± 0.65	-0.05 ± 0.05	-0.4
$\langle P_2(B \to K^*\mu^+\mu^-)\rangle_{q^2\in[2,4.3]\mathrm{GeV}^2}$	0.50 ± 0.08	0.25 ± 0.09	$+2.0$
$\langle P_4'(B \to K^*\mu^+\mu^-)\rangle_{q^2\in[2,4.3]\mathrm{GeV}^2}$	0.74 ± 0.60	0.54 ± 0.07	$+0.3$
$\langle P_5'(B \to K^*\mu^+\mu^-)\rangle_{q^2\in[2,4.3]\mathrm{GeV}^2}$	0.29 ± 0.40	-0.33 ± 0.11	$+1.5$
$\langle P_6'(B \to K^*\mu^+\mu^-)\rangle_{q^2\in[2,4.3]\mathrm{GeV}^2}$	-0.15 ± 0.38	-0.06 ± 0.06	-0.2
$\langle P_8'(B \to K^*\mu^+\mu^-)\rangle_{q^2\in[2,4.3]\mathrm{GeV}^2}$	-0.3 ± 0.60	0.04 ± 0.05	-0.6
$10^7 \langle \mathrm{dBR}/\mathrm{d}q^2(B \to K^*\mu^+\mu^-)\rangle_{q^2\in[4.3,8.68]\mathrm{GeV}^2}$	0.49 ± 0.08	0.48 ± 0.53	$+0.0$
$\langle F_L(B \to K^*\mu^+\mu^-)\rangle_{q^2\in[4.3,8.68]\mathrm{GeV}^2}$	0.57 ± 0.08	0.63 ± 0.14	-0.4
$\langle P_1(B \to K^*\mu^+\mu^-)\rangle_{q^2\in[4.3,8.68]\mathrm{GeV}^2}$	0.36 ± 0.31	-0.11 ± 0.06	$+1.5$
$\langle P_2(B \to K^*\mu^+\mu^-)\rangle_{q^2\in[4.3,8.68]\mathrm{GeV}^2}$	-0.25 ± 0.08	-0.36 ± 0.05	$+1.1$
$\langle P_4'(B \to K^*\mu^+\mu^-)\rangle_{q^2\in[4.3,8.68]\mathrm{GeV}^2}$	1.18 ± 0.32	0.99 ± 0.03	$+0.6$
$\langle P_5'(B \to K^*\mu^+\mu^-)\rangle_{q^2\in[4.3,8.68]\mathrm{GeV}^2}$	-0.19 ± 0.16	-0.83 ± 0.05	$+3.8$
$\langle P_6'(B \to K^*\mu^+\mu^-)\rangle_{q^2\in[4.3,8.68]\mathrm{GeV}^2}$	0.04 ± 0.16	-0.02 ± 0.06	$+0.4$
$\langle P_8'(B \to K^*\mu^+\mu^-)\rangle_{q^2\in[4.3,8.68]\mathrm{GeV}^2}$	0.58 ± 0.38	0.02 ± 0.06	$+1.4$
$10^7 \langle \mathrm{dBR}/\mathrm{d}q^2(B \to K^*\mu^+\mu^-)\rangle_{q^2\in[14.18,16]\mathrm{GeV}^2}$	0.56 ± 0.10	0.67 ± 1.17	-0.1
$\langle F_L(B \to K^*\mu^+\mu^-)\rangle_{q^2\in[14.18,16]\mathrm{GeV}^2}$	0.33 ± 0.09	0.39 ± 0.24	-0.2
$\langle P_1(B \to K^*\mu^+\mu^-)\rangle_{q^2\in[14.18,16]\mathrm{GeV}^2}$	0.07 ± 0.28	-0.32 ± 0.70	$+0.5$
$\langle P_2(B \to K^*\mu^+\mu^-)\rangle_{q^2\in[14.18,16]\mathrm{GeV}^2}$	-0.50 ± 0.03	-0.47 ± 0.14	-0.2
$\langle P_4'(B \to K^*\mu^+\mu^-)\rangle_{q^2\in[14.18,16]\mathrm{GeV}^2}$	-0.18 ± 0.70	1.15 ± 0.33	-1.7
$\langle P_5'(B \to K^*\mu^+\mu^-)\rangle_{q^2\in[14.18,16]\mathrm{GeV}^2}$	-0.79 ± 0.27	-0.82 ± 0.36	$+0.1$
$\langle P_6'(B \to K^*\mu^+\mu^-)\rangle_{q^2\in[14.18,16]\mathrm{GeV}^2}$	0.18 ± 0.25	0.00 ± 0.00	$+0.7$
$\langle P_8'(B \to K^*\mu^+\mu^-)\rangle_{q^2\in[14.18,16]\mathrm{GeV}^2}$	-0.40 ± 0.60	0.00 ± 0.01	-0.7
$10^7 \langle \mathrm{dBR}/\mathrm{d}q^2(B \to K^*\mu^+\mu^-)\rangle_{q^2\in[16,19]\mathrm{GeV}^2}$	0.41 ± 0.07	0.43 ± 0.78	$+0.0$
$\langle F_L(B \to K^*\mu^+\mu^-)\rangle_{q^2\in[16,19]\mathrm{GeV}^2}$	0.38 ± 0.09	0.36 ± 0.13	$+0.1$
$\langle P_1(B \to K^*\mu^+\mu^-)\rangle_{q^2\in[16,19]\mathrm{GeV}^2}$	-0.71 ± 0.36	-0.55 ± 0.59	-0.2
$\langle P_2(B \to K^*\mu^+\mu^-)\rangle_{q^2\in[16,19]\mathrm{GeV}^2}$	-0.32 ± 0.08	-0.41 ± 0.15	$+0.5$
$\langle P_4'(B \to K^*\mu^+\mu^-)\rangle_{q^2\in[16,19]\mathrm{GeV}^2}$	0.70 ± 0.52	1.24 ± 0.25	-0.9
$\langle P_5'(B \to K^*\mu^+\mu^-)\rangle_{q^2\in[16,19]\mathrm{GeV}^2}$	-0.60 ± 0.21	-0.66 ± 0.37	$+0.1$
$\langle P_6'(B \to K^*\mu^+\mu^-)\rangle_{q^2\in[16,19]\mathrm{GeV}^2}$	-0.31 ± 0.39	0.00 ± 0.00	-0.8
$\langle P_8'(B \to K^*\mu^+\mu^-)\rangle_{q^2\in[16,19]\mathrm{GeV}^2}$	0.12 ± 0.54	0.00 ± 0.04	$+0.2$

manner and with an arbitrary phase. The computation of these observables is implemented within SuperIso [39,40], and the marginal numerical differences on the SM predictions with respect to Ref. [38] are due to slightly different choice of central values for input parameters.

A visualisation of how these observables depend on the various Wilson coefficients can be obtained by linearising with respect to the NP contributions to the coefficients. In addition, New Physics contributions to the primed coefficients $\mathcal{C}'_{7,9,10}$ are always negligible in the scenarios considered in this paper, being suppressed by a factor m_s/m_b like in the SM. Within these approximations, we have

$$\begin{aligned}
\delta\langle P_2\rangle_{[0.1,2]} &\simeq +0.37\,\delta\mathcal{C}_7 +0.02\,\delta\mathcal{C}_8 && -0.03\,\delta\mathcal{C}_{10}\\
\delta\langle P_2\rangle_{[2,4.3]} &\simeq -2.48\,\delta\mathcal{C}_7 -0.10\,\delta\mathcal{C}_8 -0.17\,\delta\mathcal{C}_9 +0.03\,\delta\mathcal{C}_{10}\\
\delta\langle P_2\rangle_{[4.3,8.68]} &\simeq -0.71\,\delta\mathcal{C}_7 -0.04\,\delta\mathcal{C}_8 -0.09\,\delta\mathcal{C}_9 -0.04\,\delta\mathcal{C}_{10}\\
\delta\langle P'_4\rangle_{[0.1,2]} &\simeq +0.59\,\delta\mathcal{C}_7 && -0.08\,\delta\mathcal{C}_9 -0.13\,\delta\mathcal{C}_{10}\\
\delta\langle P'_4\rangle_{[2,4.3]} &\simeq +2.45\,\delta\mathcal{C}_7 +0.11\,\delta\mathcal{C}_8 +0.06\,\delta\mathcal{C}_9 -0.14\,\delta\mathcal{C}_{10}\\
\delta\langle P'_4\rangle_{[4.3,8.68]} &\simeq +0.33\,\delta\mathcal{C}_7 +0.01\,\delta\mathcal{C}_8 +0.01\,\delta\mathcal{C}_9\\
\delta\langle P'_5\rangle_{[0.1,2]} &\simeq -0.91\,\delta\mathcal{C}_7 -0.04\,\delta\mathcal{C}_8 -0.12\,\delta\mathcal{C}_9 -0.03\,\delta\mathcal{C}_{10}\\
\delta\langle P'_5\rangle_{[2,4.3]} &\simeq -3.04\,\delta\mathcal{C}_7 -0.14\,\delta\mathcal{C}_8 -0.29\,\delta\mathcal{C}_9 -0.03\,\delta\mathcal{C}_{10}\\
\delta\langle P'_5\rangle_{[4.3,8.68]} &\simeq -0.52\,\delta\mathcal{C}_7 -0.03\,\delta\mathcal{C}_8 -0.08\,\delta\mathcal{C}_9 -0.03\,\delta\mathcal{C}_{10}
\end{aligned} \tag{2.6}$$

while the rest of the observables are less sensitive to real NP contributions in $\mathcal{C}_{7,8,9,10}$:

$$\begin{aligned}
\delta\langle P'_6\rangle_{[0.1,2]} &\simeq -0.21\,\delta\mathcal{C}_7 +0.09\,\delta\mathcal{C}_8\\
\delta\langle P'_6\rangle_{[2,4.3]} &\simeq -0.07\,\delta\mathcal{C}_7 +0.09\,\delta\mathcal{C}_8\\
\delta\langle P'_6\rangle_{[4.3,8.68]} &\simeq +0.02\,\delta\mathcal{C}_7 +0.04\,\delta\mathcal{C}_8\\
\delta\langle P'_8\rangle_{[0.1,2]} &\simeq +0.20\,\delta\mathcal{C}_7 -0.11\,\delta\mathcal{C}_8 +0.01\,\delta\mathcal{C}_9\\
\delta\langle P'_8\rangle_{[2,4.3]} &\simeq +0.11\,\delta\mathcal{C}_7 -0.10\,\delta\mathcal{C}_8 +0.01\,\delta\mathcal{C}_9 +0.02\,\delta\mathcal{C}_{10}\\
\delta\langle P'_8\rangle_{[4.3,8.68]} &\simeq +0.01\,\delta\mathcal{C}_7 -0.04\,\delta\mathcal{C}_8
\end{aligned} \tag{2.7}$$

and P_1 depends (almost) only on right-handed currents. In addition, the observables P'_5 and P'_6 depend formally on scalar operators through the combination $(\mathcal{C}_{Q_1} - \mathcal{C}'_{Q_1})$. However, the coefficient in the linearised expression is smaller than 0.01 and has been neglected. We recall that the coefficients $\delta\mathcal{C}_i$ are defined at the scale m_b.

The strongest constraint on $\delta\mathcal{C}_7$ is provided by the branching ratio $\mathrm{BR}(B \to X_s\gamma)$, which strongly favours values around $\delta\mathcal{C}_7 \in (-0.07, 0.04)$, with preference for negative values. Looking at Eqs. (2.6) one can see that such negative small contributions to $\mathcal{C}_7$ tend to increase the theory predictions for $\langle P_2\rangle_{[2,4.3]}$, $\langle P_2\rangle_{[4.3,8.68]}$, $\langle P'_5\rangle_{[2,4.3]}$, $\langle P'_5\rangle_{[4.3,8.68]}$ and decrease the value of $\langle P_2\rangle_{[0.1,2]}$, improving the agreement with experiment. On the other hand the contributions to $\langle P'_5\rangle_{[0.1,2]}$ and $\langle P'_4\rangle$ go in the opposite direction, although still compatible within errors (experimental uncertainties on P'_4 are still rather large). Therefore, these observables will generally drift $\delta\mathcal{C}_7$ towards small negative values in agreement with the expectations from $\mathrm{BR}(B \to X_s\gamma)$ (see Ref. [1] and Fig. 5 therein).

However, in order to explain the observable $\langle P'_5\rangle_{[4.3,8.68]}$, and to a lesser extent also $\langle P_2\rangle_{[4.3,8.68]}$ and $\langle P'_5\rangle_{[2,4.3]}$, the contributions to other Wilson coefficients are necessary. As can be seen from Eqs. (2.6), the sensitivity to $\delta\mathcal{C}_{10}$ is lower than to $\delta\mathcal{C}_9$, so the latter is the best candidate. In addition, $\delta\mathcal{C}_{10}$ is constrained by $\mathrm{BR}(B_s \to \mu^+\mu^-)$ to an extent that depends on the pattern of scalar contributions. In the MSSM (where $\mathcal{C}_{Q_1} \approx -\mathcal{C}_{Q_2}$) this constraint is very effective. In this context it was shown in Ref. [1] that the most favourable scenario involves a significant negative contribution to $\mathcal{C}_9$.

Such large NP contributions to $\mathcal{C}_9$ are not possible in general within the MSSM (see also Ref. [2]) and, as we shall see, moderately large negative values for $\delta\mathcal{C}_9$—achievable within corners of the pMSSM—are typically correlated to large values of other coefficients that lead to tensions with other flavour data. However, we will also see that all $B \to K^*\mu^+\mu^-$ observables including $\langle P_2\rangle_{[4.3,8.68]}$ and $\langle P'_5\rangle_{[2,4.3]}$ can be well described within the pMSSM, except for $\langle P'_5\rangle_{[4.3,8.68]}$, which remains a challenge.

3 MSSM scenarios

We consider two classes of scenarios: the constrained MSSM scenarios CMSSM and NUHM, and a more general set-up with no universality assumptions for the sparticle masses at a high scale: the phenomenological MSSM (pMSSM) [54]. We scan over the parameters of the MSSM scenarios using SOFTSUSY 3.3.10 [45] in the ranges given in Table 2, and we generate several millions of random points for each scenario. For each generated point, we then calculate the flavour observables with SuperIso v3.4 [39,40]. We apply a few loose cuts for some of the SUSY masses to avoid regions of the parameters that are excluded by direct SUSY searches. In particular we impose the gluino and squark masses to be above 500 GeV and the chargino masses above 150 GeV. These limits could be much stronger in the CMSSM, but since the strong CMSSM limits are falsified in the case of pMSSM (see Ref. [55]) we consider the same loose cuts for all the scenarios we analyse here.

4 Statistical method

In order to study the overall compatibility of the MSSM scenarios with the $B \to K^*\mu^+\mu^-$ measurements, including all other relevant flavour constraints, we perform a statistical χ^2 analysis of the data. We consider all 45 observables collected in Table 1 and construct the χ^2 distribution:

$$\chi^2 = \sum_{\text{bins}} \left[\sum_{j,k\in(B\to K^*\mu^+\mu^-\ \text{obs.})} \left(O_j^{\text{exp}} - O_j^{\text{th}}\right)\left(\sigma^{(\text{bin})}\right)^{-1}_{jk} \times\left(O_k^{\text{exp}} - O_k^{\text{th}}\right)\right] + \sum_{i\in(\text{other obs.})} \frac{\left(O_i^{\text{exp}} - O_i^{\text{th}}\right)^2}{\left(\sigma_i^{\text{exp}}\right)^2 + \left(\sigma_i^{\text{th}}\right)^2}, \tag{4.1}$$

Table 2 Parameter ranges adopted in the scans (in GeV when applicable) for the CMSSM, NUHM and pMSSM scenarios

CMSSM parameter	Range
$\tan\beta$	[2, 60]
m_0	[50, 3,000]
$m_{1/2}$	[50, 3,000]
A_0	[−10,000, 10,000]
$\mathrm{sgn}(\mu)$	±
NUHM parameter	**Range**
$\tan\beta$	[2, 60]
m_0	[50, 3,000]
$m_{1/2}$	[50, 3,000]
m_A	[50, 3,000]
A_0	[−10,000, 10,000]
μ	[−5,000, 5,000]
pMSSM parameter	**Range**
$\tan\beta$	[2, 60]
M_A	[50, 3,000]
M_1	[50, 3,000]
M_2	[50, 3,000]
M_3	[50, 3,000]
$A_d = A_s = A_b$	[−10,000, 10,000]
$A_u = A_c = A_t$	[−10,000, 10,000]
$A_e = A_\mu = A_\tau$	[−10, 000, 10,000]
μ	[−5, 000, 5,000]
$M_{\tilde{e}_L} = M_{\tilde{\mu}_L}$	[50, 3,000]
$M_{\tilde{e}_R} = M_{\tilde{\mu}_R}$	[50, 3,000]
$M_{\tilde{\tau}_L}$	[50, 3,000]
$M_{\tilde{\tau}_R}$	[50, 3,000]
$M_{\tilde{q}_{1L}} = M_{\tilde{q}_{2L}}$	[50, 3,000]
$M_{\tilde{q}_{3L}}$	[50, 3,000]
$M_{\tilde{u}_R} = M_{\tilde{c}_R}$	[50, 3,000]
$M_{\tilde{t}_R}$	[50, 3,000]
$M_{\tilde{d}_R} = M_{\tilde{s}_R}$	[50, 3,000]
$M_{\tilde{b}_R}$	[50, 3,000]

where the central value of the experimental result and theoretical prediction of observable i are given in O_i^{exp} and O_i^{th}, respectively. The first term contains the contribution to the χ^2 from the $B \to K^*\mu^+\mu^-$ observables. Here we include the experimental correlations among the $B \to K^*\mu^+\mu^-$ observables, and the inverse of the correlation matrices $(\sigma^{(\mathrm{bin})})^{-1}$ for each bin are taken from [4,56]. The second term is the standard χ^2 without correlations for all the other observables. σ_i^{exp} and σ_i^{th} are the experimental and theoretical errors, respectively. Each MSSM point (defining a particular *model*) is therefore assigned a χ^2 value, which is directly related to the p-value of the model: the probability that another measurement of these observables leads to worse agreement with the model predictions, assuming the model is true. All models with p-values greater than $\hat{p}$ lie inside a $(1-\hat{p})\times 100$ % C.L. region. One-, two- and three-sigma regions are defined as the 68.3, 95.4 and 99.7 % C.L. regions, respectively. Note that this approach is different from the one used in e.g. Refs. [1,28] as well as from the Bayesian procedure in Refs. [3,25,26] where the difference of the χ^2 for each point with the χ^2 of the best fit point ($\Delta\chi^2$) is used to define the different allowed regions, but it is similar to the method of Ref. [4].

Here we are not aiming to determine a preferred direction to which the current results with the observed anomalies would point to, but instead our goal is to examine the global agreement of the data with the MSSM predictions. Hence the use of the absolute χ^2 method is justified. Note, however, that if we had used the $\Delta\chi^2$ method instead, we could still find solutions at the 1σ level, certainly different from the $\delta\mathcal{C}_9 \sim -1$ benchmark, because this method relies on finding a *best fit point* regardless of the goodness-of-fit of this point, and it depends on the model parameter ranges. On the contrary, in the absolute χ^2 method the allowed regions are defined directly from the value of the χ^2 as explained above, and they are independent of the parameter ranges.

5 Results

5.1 MSSM predictions for $B \to K^*\mu^+\mu^-$ observables

We study first the reach of each MSSM scenario for all $B \to K^*\mu^+\mu^-$ observables, without applying any flavour or Higgs mass constraint. In this case the parameter space in each model is large enough to contribute significantly to each observable. The most interesting observables, P_2, P_4' and P_5', are shown in Fig. 1, where the bands show the span of values allowed in this set-up. For comparison also the experimental results are shown (black data points), together with the SM central values (red line). As can be seen from the figure all MSSM scenarios can explain, within 1σ, each *individual* tension for all observables.[1] Any tension between the MSSM and $B \to K^*\mu^+\mu^-$ data can only come from correlations among this data, or from the combination with other constraints.

One such independent constraint is the Higgs mass. In order to see the effect of this constraint, we impose the condition $121 < M_h < 129$ GeV [57,58] on the scan points in each MSSM scenario. The MSSM contributions to $B \to K^*\mu^+\mu^-$ observables are slightly reduced, as can

[1] Note that $\langle P_4' \rangle$ at low recoil cannot be changed by any significant amount since in this kinematic region this observable is independent of short distance physics, so that in particular the tension in the bin [14.18, 16] GeV^2 cannot be explained by New Physics.

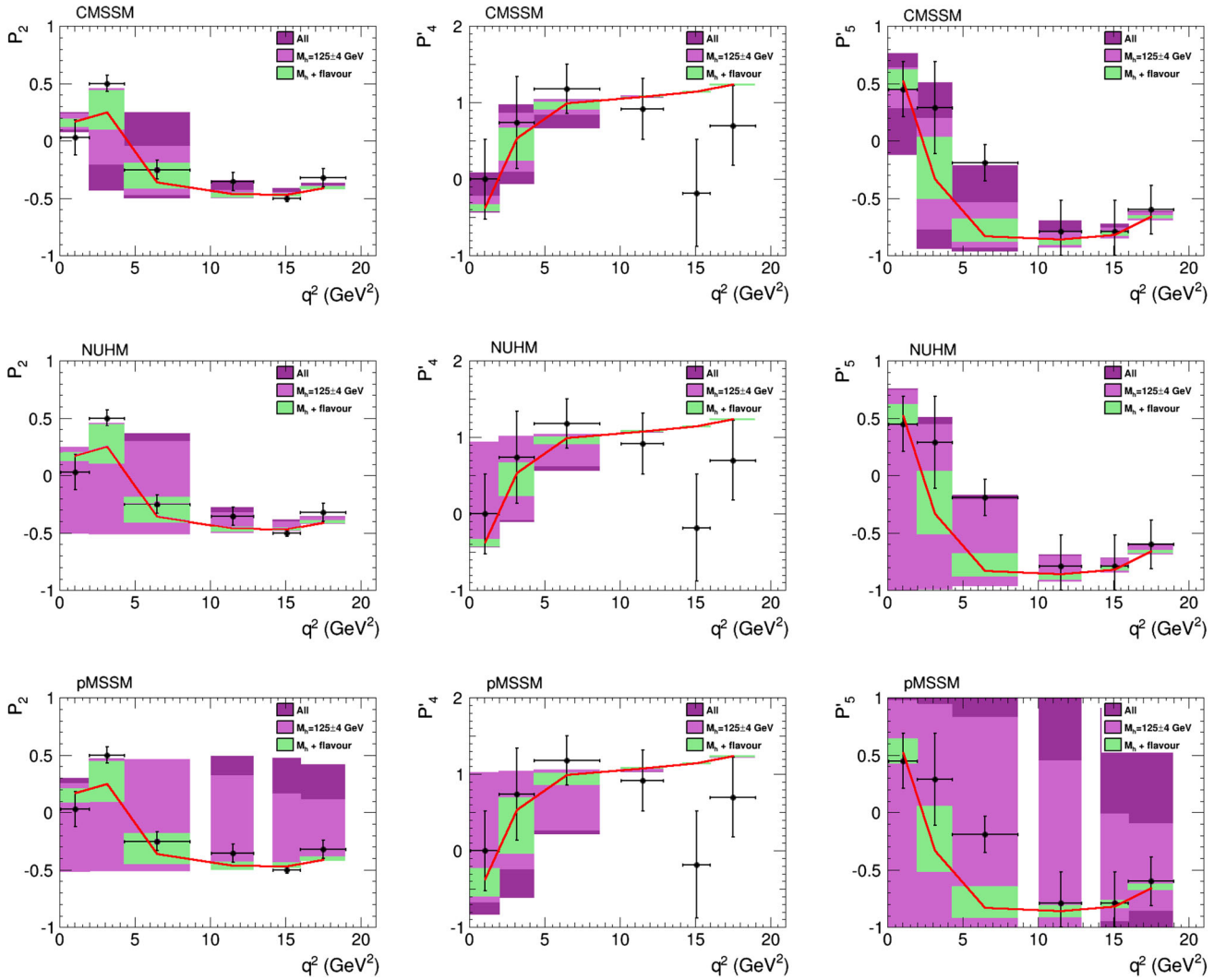

Fig. 1 MSSM predictions for P_2 (*left*), P_4' (*centre*) and P_5' (*right*) within the CMSSM (*upper row*), NUHM (*central row*) and pMSSM (*lower row*). The *dark purple* regions correspond to the full predictions while the *light purple* zones are obtained after applying the Higgs mass constraints. The *green* bands include all flavour constraints (see Sect. 5.2)

be seen in Fig. 1, where the light purple bands show the span of values allowed from MSSM points satisfying the Higgs mass constraint. This reduction is inconsequential for all observables (again, barring possible correlations), except for $\langle P_5' \rangle_{[4.3,8.68]}$, where one-sigma agreement is impossible in the constrained scenarios. The pMSSM on the other hand is general enough to provide solutions at the 1σ level.

On the basis of these results, the relevant issue is how these observables are correlated in the different MSSM scenarios, among themselves and with other flavour observables. Even though Fig. 1 looks promising, the region in MSSM parameter space where a good agreement is found for e.g. $\langle P_2 \rangle_{[2,4.3]}$, could be predicting unacceptable values for $\langle P_5' \rangle_{[2,4.3]}$, or for other observables such as $\mathrm{BR}(B \to X_s\gamma)$. In this respect this is the main characteristic feature of a model-dependent analysis in contrast to a model-independent one where the various Wilson coefficients are independent parameters: correlations can lead to completely different global patterns even when the range of values for the Wilson coefficients are fixed.

We consider first several interesting examples of correlations among different observables within the MSSM. Even in a model-independent set-up, where all Wilson coefficients are treated as independent free parameters, strong correlations among different observables are present. In the MSSM and in the case of small contributions to $\delta\mathcal{C}_9$, sufficiently large values of $\delta\mathcal{C}_7$ can enhance the relevant $B \to K^*\mu^+\mu^-$ observables enough to match the data. Irrespectively of whether these values are correlated to other Wilson coefficients, these large values of $\delta\mathcal{C}_7$ are in tension with the measurement of $\mathrm{BR}(B \to X_s\gamma)$. This is a (known) model-independent statement [1,28]. With values for the Wilson coefficients reachable in the MSSM, the observables

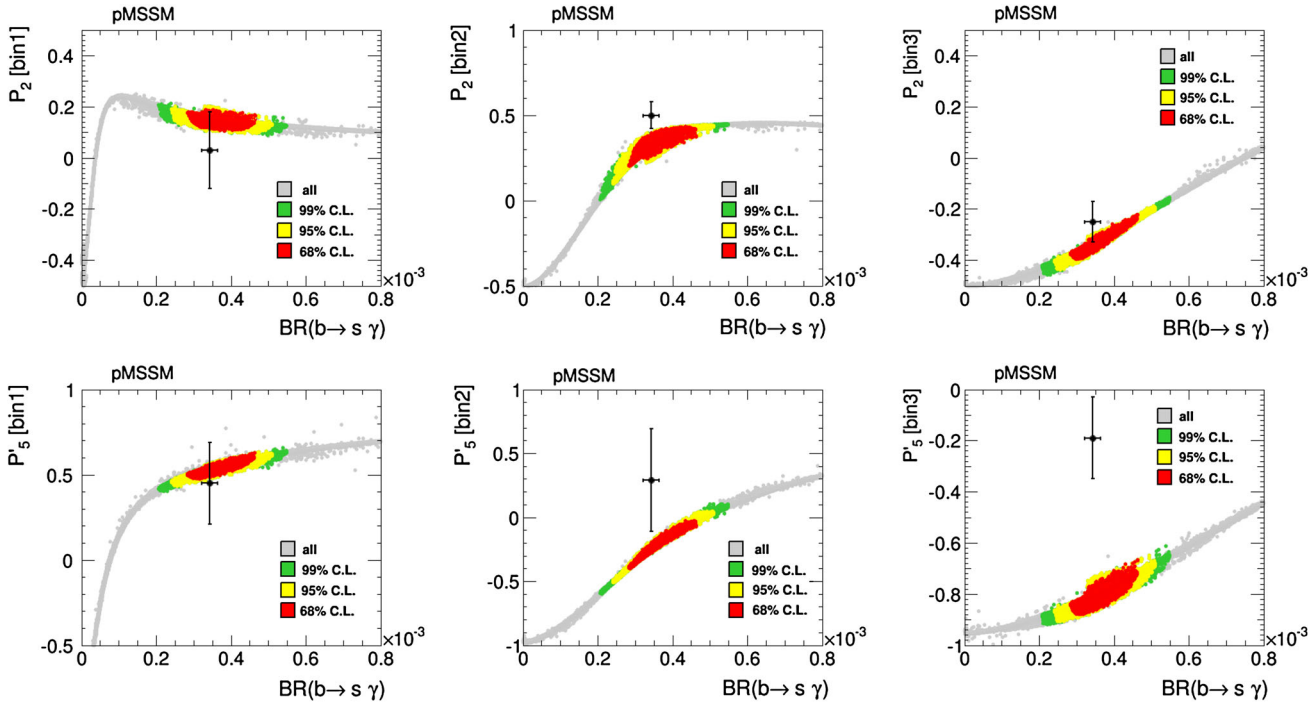

Fig. 2 Correlations among P_2 and P_5' in the first three low q^2 bins and $\mathrm{BR}(B \to X_s\gamma)$ in pMSSM. The *black data points* and *error bars* represent the experimental measurements

$\langle P_2\rangle_{[2,4.3]}$, $\langle P_5'\rangle_{[2,4.3]}$ and $\langle P_5'\rangle_{[4.3,8.68]}$ can acquire large values in agreement with data; however this is mainly due to contributions to $\delta\mathcal{C}_7$ that enhance $\mathrm{BR}(B \to X_s\gamma)$ – up to unacceptable levels in the case of $\langle P_5'\rangle_{[4.3,8.68]}$ (see Fig. 2). One has then to reach a statistical compromise between these two competing tensions, in order to decide whether $\delta\mathcal{C}_7$ is more likely enhanced or not. Nevertheless, this tension will lead to a global enhancement of the χ^2, and again the statistical framework will tell if this enhancement is admissible or not, in the latter case ruling out the corresponding MSSM scenario according to some statistical criteria. We should note, however, that both $B \to X_s\gamma$ and $B \to K^*\mu^-\mu^+$ observables show a preference for negative values of $\delta\mathcal{C}_7$ (albeit to different degrees) which is by itself an intriguing fact.

In the model-independent framework, this tension can be cured in part with sizeable contributions to $\mathcal{C}_9$, although it can never provide a good description of $\langle P_5'\rangle_{[4.3,8.68]}$, at least without contributions to $\mathcal{C}_9'$ [1]. In the MSSM, not only we have no means of generating any sizeable contribution to the coefficient $\mathcal{C}_9'$, but also any significant contribution to $\mathcal{C}_9$ is correlated to contributions to other Wilson coefficients affecting the other observables. Some of these interesting patterns are shown in Fig. 2.

5.2 Constraints on the Wilson coefficients

The flavour observables depend on the MSSM parameters only through the Wilson coefficients, and so it is the case for the χ^2 distribution. It is therefore quite convenient to look at the models and their C.L. regions in the space of Wilson coefficients. This is shown in Fig. 3, where all the points in the scans are shown (grey), indicating the values for the Wilson coefficients allowed within the MSSM, as well as the points satisfying the global 1, 2, 3 σ (red, yellow, green). The Higgs mass constraint has also been imposed, all the points being consistent with a Higgs mass $121 < M_h < 129$ GeV.

The comparison with the model-independent fit in Ref. [1] as well as with Refs. [2,3] is not straightforward.[2] In particular, the results in Fig. 3 do not contradict the result of Ref. [1] that a scenario with $\delta\mathcal{C}_9 \sim -1.2$ and $\delta\mathcal{C}_7 \sim -0.1$ is the most favourable one and with respect to which the SM hypothesis has a pull of ~ 3–$4\,\sigma$. Notice that: (a) no such large values for $\delta\mathcal{C}_9$ are allowed within these MSSM scenarios, and (b) even though the χ^2 grows for $\delta\mathcal{C}_9$ decreasing from ~ -0.2 (at least within the limited number of scan points, see the centre plot in the last row of Fig. 3), these points lead simultaneously to values for other Wilson coefficients away from zero, and therefore they cannot be compared with a model-independent analysis where $\delta\mathcal{C}_9$ can be decreased independently of the values of the other coefficients. As mentioned earlier, this is the

[2] The reason is due to the different statistical approaches used as explained in Sect. 4, and also to the different sets of effective operators (we also consider the effect of $\mathcal{O}_8$ in our analysis while the chirarity flipped operator effects are negligible in MSSM).

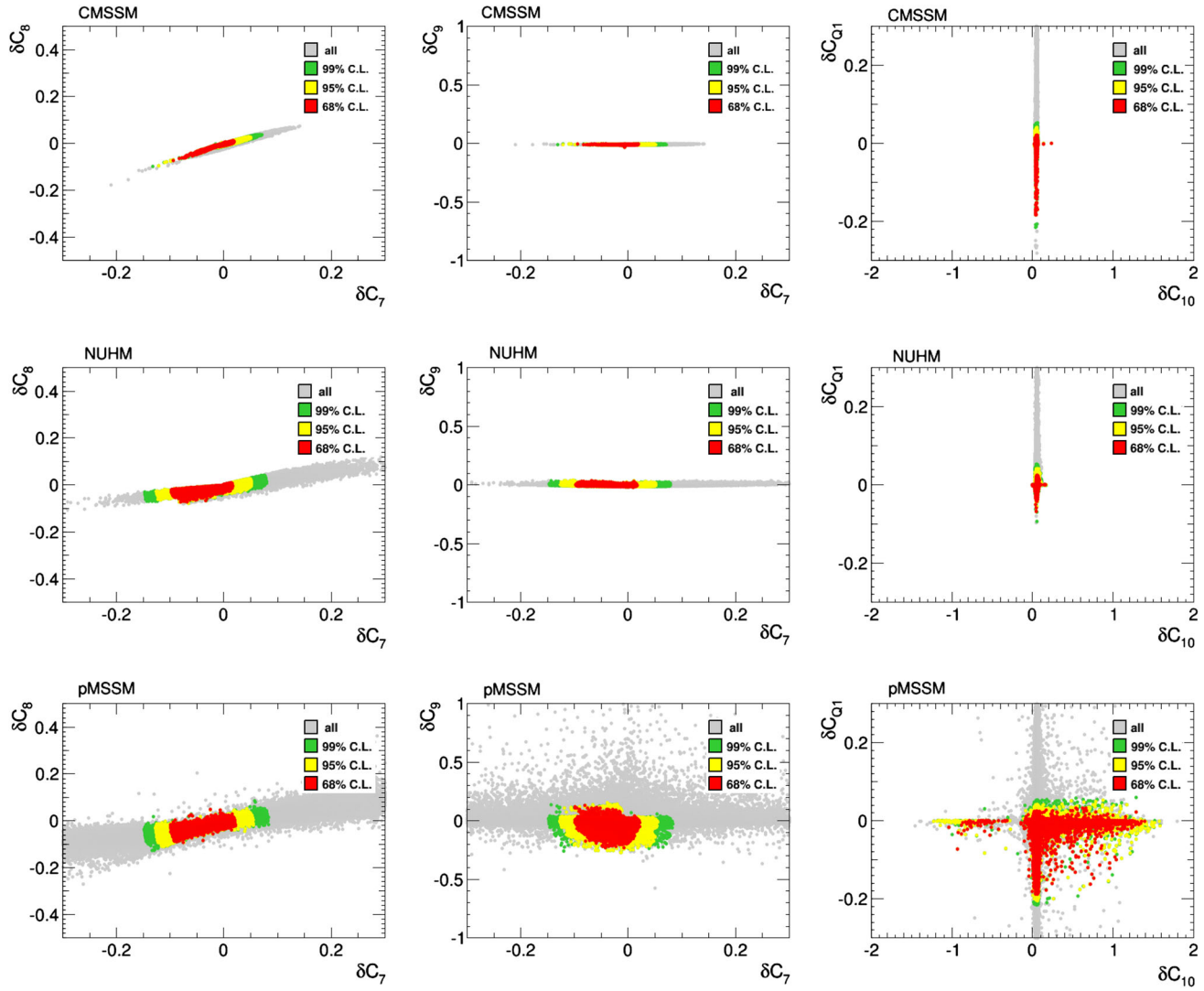

Fig. 3 Global fit to the NP coefficients $\delta\mathcal{C}_i$ at the μ_b scale in CMSSM (*upper row*), in NUHM (*central row*) and in pMSSM (*lower row*), at 68% C.L. (*red*) and 95% C.L. (*yellow*) and 99% C.L. (*green*) using the observables given in Table 1, including the Higgs mass constraint

result of strong model-dependent correlations absent within the model-independent approach.

As a conclusion, the most favourable MSSM models given the $B \to K^*\mu^+\mu^-$ data lead only to small deviations for the Wilson coefficients with respect to their SM values. The best scenarios in terms of Wilson coefficients, known from model-independent analyses, are not reachable within the constrained MSSM models, or even within the more generous pMSSM. However, the overall agreement is fairly good, with regions in SUSY parameter space where the absolute χ^2 is sufficiently small. With these statistical criteria the MSSM is still well compatible with the data.

It is instructive to go back to Fig. 1 and impose the constraints derived from the global fit. This is shown as the overimposed green bands, showing the span of models that survive the $1\,\sigma$ constraints from the global fit. We see that good agreement with $\langle P_2\rangle_{[2,4.3]}$ and $\langle P_5'\rangle_{[2,4.3]}$ can be obtained, improving the situation with respect to the SM. On the other hand, the tension in $\langle P_5'\rangle_{[4.3,8.68]}$ cannot be explained within the pMSSM. This is compatible with the previous observation that, without significant contributions to $\mathcal{C}_9$, a large value for $\langle P_5'\rangle_{[4.3,8.68]}$ requires extreme values for other Wilson coefficients that, while reachable within the MSSM, are ruled out by other flavour bounds.

5.3 Implications for MSSM parameters

The results of the global fit can be used to put constraints on the supersymmetric parameters. This is done by computing such quantities from the input parameters within each MSSM scenario which satisfies the global constraints in the fit.

First, in order to see the impact of the newly measured $B \to K^*\mu^+\mu^-$ observables in a simple framework, in Fig. 4 we compare the constraining power of the fit to

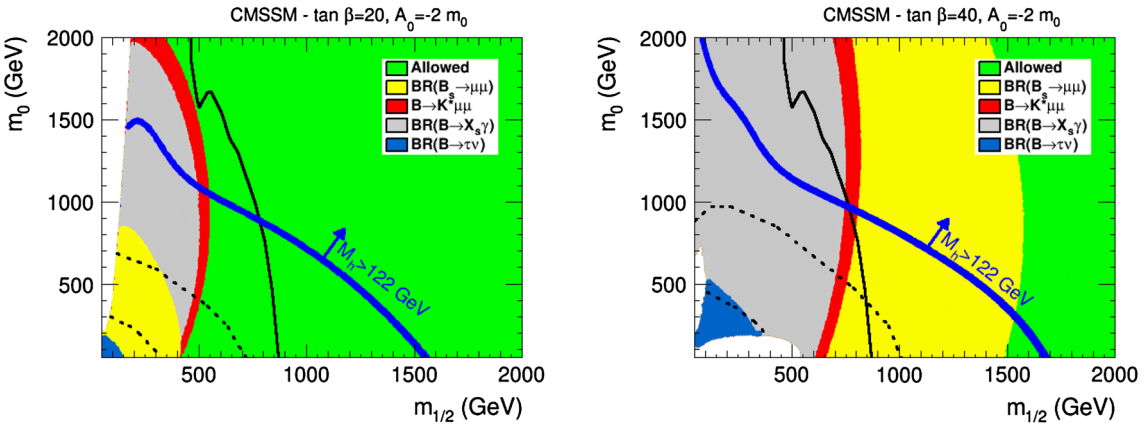

Fig. 4 Flavour constraints in CMSSM in the plane $(m_{1/2}, m_0)$ for $A_0 = -2m_0$ and $\tan\beta = 20$ (*left*) and 40 (*right*). The *black line* represents the experimental direct SUSY search limit with 20.3 fb^{-1} of data at 8 TeV [59]. The region between *dotted black lines* would explain the muon anomalous magnetic moment a_μ

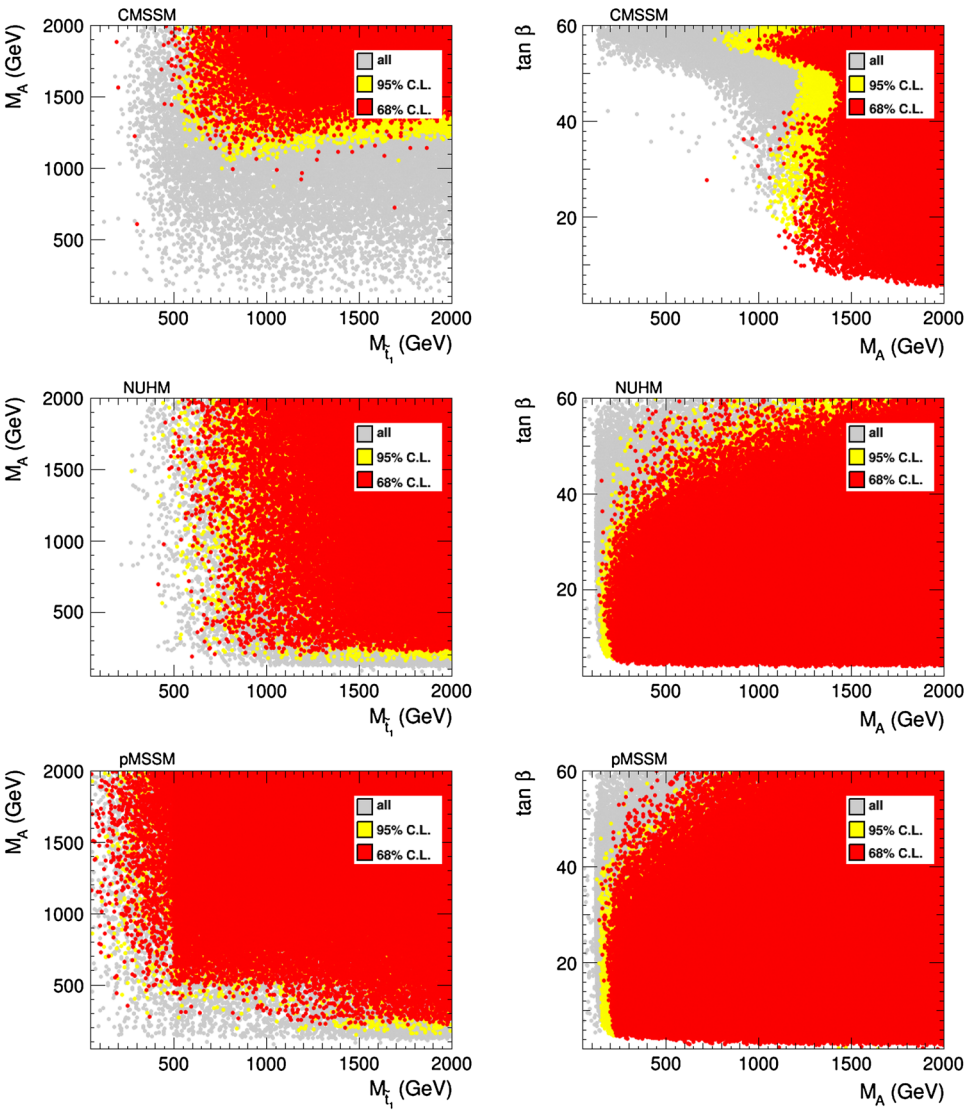

Fig. 5 Allowed regions at 68 % C.L. (*red*) and 95 % C.L. (*yellow*) in the planes $(M_{\tilde{t}_1}, M_A)$ (*left*) and $(M_A, \tan\beta)$ (*right*) in CMSSM (*upper row*), in NUHM (*central row*) and in pMSSM (*lower row*)

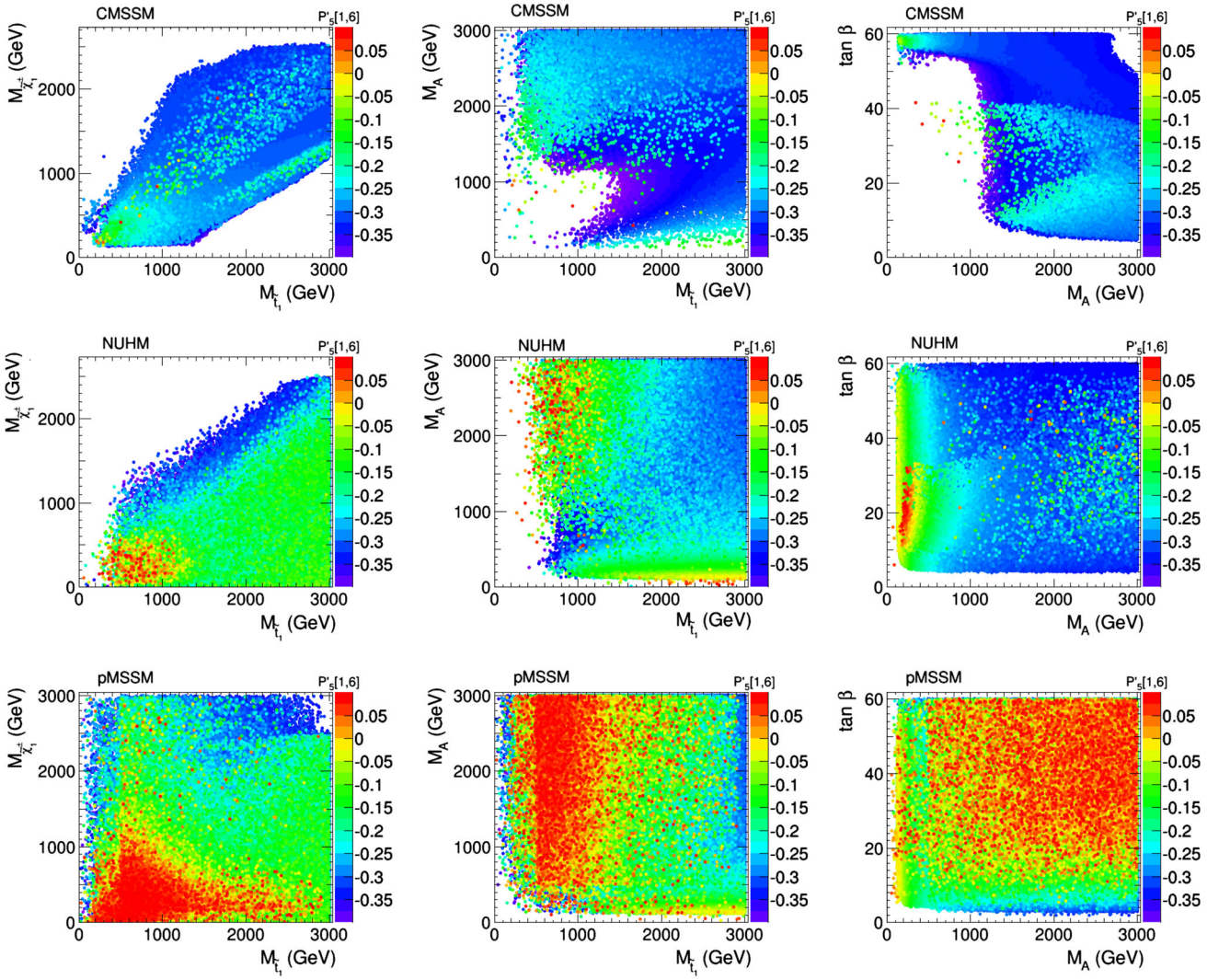

Fig. 6 Intensity of P_5' in the [1, 6] GeV bin in colour scale, in the planes $(M_{\tilde{t}_1}, M_{\tilde{\chi}_1^\pm})$ (*left*), $(M_{\tilde{t}_1}, M_A)$ (*centre*) and $(M_A, \tan\beta)$ (*right*) in CMSSM (*upper row*), in NUHM (*central row*) and in pMSSM (*lower row*). The SM prediction for P_5' in the [1, 6] GeV bin is -0.34 ± 0.10, and the experimental result is $0.21 \pm 0.21 \pm 0.03$

$B \to K^*\mu^+\mu^-$ observables with some of the other flavour observables (i.e. the Branching Ratios of $B_s \to \mu^+\mu^-$, $B \to X_s\gamma$ and $B \to \tau\nu$) in the CMSSM. We have kept $\tan\beta$ to the fixed values of 20 and 40 and the trilinear soft breaking parameter $A_0 = -2m_0$ (this choice allows us to have better agreement with the Higgs mass). In this way, the results in the two dimensional $(m_{1/2}, m_0)$ plane can easily be understood. The constraints from the combination of $B \to K^*\mu^+\mu^-$ observables are shown in red and can be compared to other flavour constraints shown in different colours according to the legends in the plots. It is remarkable that the constraints from $B \to K^*\mu^+\mu^-$ using the recent measurements are at the same level as the ones from the well-known BR$(B \to X_s\gamma)$ constraints. Also, the constraints from $B_s \to \mu^+\mu^-$ while being very strong at large $\tan\beta$, are less restrictive for lower values of $\tan\beta$ where the $B \to K^*\mu^+\mu^-$ constraints dominate. For comparison we show also in the figure the direct SUSY search limits in the same plane from ATLAS with 20.3 fb^{-1} of data at $\sqrt{s} = 8$ TeV [59], as well as the region where the Higgs mass is above 122 GeV. It is also very interesting to notice that the flavour constraints start being stronger than the direct search limits for large values of $\tan\beta \gtrsim 20$.

In very constrained scenarios such as the CMSSM, other observables are correlated to the ones studied in this paper. One example is the anomalous magnetic moment of the muon a_μ. It is well known that the discrepancy in a_μ is difficult to explain in the CMSSM, requiring low values for $m_0, m_{1/2}$ virtually excluded by LHC data [60,61]. The corresponding constraints are shown in Fig. 4, where the allowed region is the one between the dotted black lines. One can see that this region is not in agreement with the Higgs mass limit.

This does not happen in the less constrained scenarios, where the leptonic and the quark sectors are mostly independent. Other observables in tension with the SM are the excess of $\bar{B} \to \bar{D}\tau^-\bar{\nu}_\tau$ and $\bar{B} \to \bar{D}^*\tau^-\bar{\nu}_\tau$ decays observed by the BaBar collaboration [62]. The excess of these decays can each be individually described in the type-II 2HDM. However, when combined, the $\bar{B} \to \bar{D}^{(*)}\tau^-\bar{\nu}_\tau$ decays exclude the type-II 2HDM charged boson at 99.8 % confidence level for any value of $\tan\beta/m_{H^+}$ [62,63]. The MSSM contributions to these two flavour changing charged current processes are also completely dominated by the exchange of a charged Higgs boson, leading to a pattern very similar to that of the type-II 2HDM. However, the other MSSM parameters have negligible contributions and are not directly constrained by the $\bar{B} \to \bar{D}^{(*)}\tau^-\bar{\nu}_\tau$ decays. We do not consider the anomalous magnetic moment of the muon and the $\bar{B} \to \bar{D}^{(*)}\tau^-\bar{\nu}_\tau$ decays any further in this paper as these observables are either impossible to reconcile with very constrained SUSY scenarios, or not of relevance to the impact of $b \to s$ constraints.

Next we consider the MSSM scenarios in full generality without fixing any parameters. The constraints from the $b \to s$ global fit on the physical parameters $M_{\tilde{t}_1}$, M_A and $\tan\beta$ are shown in Fig. 5. Several interesting features can be observed. First, while the constraints are very strong in the CMSSM, they can easily be relaxed in the more general scenarios NUHM or pMSSM. In the case of the CMSSM, the pseudo-scalar Higgs mass is constrained quite generally to be above $\sim$1 TeV. This strong limit from flavour physics is independent of the value of $\tan\beta$. Another interesting feature is the impact on the lightest stop mass. In the constrained scenarios, flavour constraints require the lightest stop to be heavier than $\sim$500 GeV. On the other hand, in the pMSSM the flavour constraints are much weaker, excluding only scenarios where M_A and $M_{\tilde{t}_1}$ are both small, or with light M_A and large $\tan\beta$.

Finally, we give special attention to P_5', as this is the only observable presenting more than 2σ tension in the MSSM, and study how the value of the observable $\langle P_5' \rangle_{[1,6]}$ changes as a function of the MSSM parameters. The results are displayed in Fig. 6. As can be seen, the tension with respect to the experimental result is reduced for small chargino or stop masses, while the other SUSY parameters are less relevant.

6 Conclusions

The angular distribution of the decay $B \to K^*\mu^+\mu^-$ provides a large number of observables, probing NP in a complementary way to other related flavour processes. This exclusive mode is under good theoretical control, with the main hadronic uncertainties stemming from the form factors and (at large recoil) unknown power corrections. In this context the use of *optimised* observables such as the set $\{P_i^{(\prime)}\}$ is very convenient in phenomenological analyses.

Recent LHCb measurements of these optimised observables have shown certain discrepancies with SM predictions, specifically in some of the P_2 and P_5' bins. Model-independent global fits for the Wilson coefficients have shown that the tensions can be relaxed if $\delta\mathcal{C}_9 \sim -1$, even if such a large $\delta\mathcal{C}_9$ is not necessarily required to find global agreement with the full set of $b \to s$ data. In this paper we have studied the implications of the new $B \to K^*\mu^+\mu^-$ results along with other relevant $b \to s$ transitions on several MSSM scenarios: the constrained CMSSM and NUHM scenarios and also the more general pMSSM framework. While large negative contributions to $\mathcal{C}_9$ are not accessible within the MSSM, it is interesting to note that the MSSM has the potential to reproduce each of the measurements individually at the $1\,\sigma$ level. Correlations among the different observables are then the central issue.

In order to study the impact of the recent LHCb results, we have first performed a global fit to the Wilson coefficients, including most of the available $b \to s$ modes. The comparison of this analysis with previous model-independent analyses is not straightforward, but can be understood in terms of model-dependent correlations (as the Wilson coefficients are correlated in MSSM and cannot be varied independently) and a different statistical set-up. In our analysis, the best fit values for the Wilson coefficients not only depend on the correlations among the different flavour observables but also on the correlations between the various Wilson coefficients in each specific MSSM scenario. Even though the small value of $\mathcal{C}_9 \sim 3$ favourable from model-independent analyses is not accessible within MSSM, there are regions of the MSSM parameter space that are still well compatible with the experimental data. Our results for the Wilson coefficients are consistent subsets of the solutions found in [4].

We have translated the constraints on different SUSY parameters in the three aforementioned scenarios. These constraints provide complementary information to direct searches and show that the data on $B \to K^*\mu^+\mu^-$ has become competitive with the traditional modes such as $B \to X_s\gamma$ and $B_s \to \mu^+\mu^-$.

The observable P_5' remains nevertheless a challenge for SUSY models. We have shown its dependence on some of the more relevant SUSY parameters, making it possible to easily look for the preferred region of parameter space within the mentioned MSSM scenarios when experimental updates on P_5' are available. We are looking forward to the experimental update including the full 3 fb^{-1} data-set collected at LHCb.

Acknowledgments We would like to thank J. Matias for valuable contributions concerning the SM predictions of $B \to K^*\mu^+\mu^-$ observables, and T. Hurth for innumerable useful discussions. J.V. is funded by the Deutsche Forschungsgemeinschaft (DFG) within research unit FOR 1873 (QFET).

References

1. S. Descotes-Genon, J. Matias, J. Virto, Phys. Rev. D **88**, 074002 (2013). arXiv:1307.5683 [hep-ph]
2. W. Altmannshofer, D.M. Straub. arXiv:1308.1501 [hep-ph]
3. F. Beaujean, C. Bobeth, D. van Dyk. arXiv:1310.2478 [hep-ph]
4. T. Hurth, F. Mahmoudi, JHEP **1404**, 097 (2014). arXiv:1312.5267 [hep-ph]
5. R.R. Horgan, Z. Liu, S. Meinel, M. Wingate. arXiv:1310.3887 [hep-ph]
6. R.R. Horgan, Z. Liu, S. Meinel, M. Wingate. arXiv:1310.3722 [hep-lat]
7. R. Gauld, F. Goertz, U. Haisch. arXiv:1308.1959 [hep-ph]
8. A.J. Buras, J. Girrbach, JHEP **1312**, 009 (2013). arXiv:1309.2466 [hep-ph]
9. R. Gauld, F. Goertz, U. Haisch. arXiv:1310.1082 [hep-ph]
10. A. Datta, M. Duraisamy, D. Ghosh. arXiv:1310.1937 [hep-ph]
11. C. Hambrock, G. Hiller, S. Schacht, R. Zwicky. arXiv:1308.4379 [hep-ph]
12. R. Aaij et al. [LHCb Collaboration], JHEP **1308**, 131 (2013). arXiv:1304.6325 [hep-ex]
13. R. Aaij et al. [LHCb Collaboration], Phys. Rev. Lett. **111**, 191801 (2013). arXiv1308.1707 [hep-ex]
14. S. Chatrchyan et al. [CMS Collaboration], Phys. Rev. Lett. **111**, 101804 (2013). arXiv:1307.5025 [hep-ex]
15. R. Aaij et al. [LHCb Collaboration], Phys. Rev. Lett. **111**, 101805 (2013). arXiv:1307.5024 [hep-ex]
16. G. Aad et al. [ATLAS Collaboration], ATLAS-CONF-2013-038, ATLAS-COM-CONF-2013-043
17. W. Altmannshofer, P. Ball, A. Bharucha, A.J. Buras, D.M. Straub, M. Wick, JHEP **0901**, 019 (2009). arXiv:0811.1214
18. C. Bobeth, M. Misiak, J. Urban, Nucl. Phys. B **574**, 291 (2000). hep-ph/9910220
19. C. Bobeth, P. Gambino, M. Gorbahn, U. Haisch, JHEP **0404**, 071 (2004). hep-ph/0312090
20. M. Misiak, M. Steinhauser, Nucl. Phys. B **683**, 277 (2004). hep-ph/0401041
21. M. Gorbahn, U. Haisch, Nucl. Phys. B **713**, 291 (2005). hep-ph/0411071
22. M. Gorbahn, U. Haisch, M. Misiak, Phys. Rev. Lett. **95**, 102004 (2005). hep-ph/0504194
23. T. Huber, E. Lunghi, M. Misiak, D. Wyler, Nucl. Phys. B **740**, 105 (2006). hep-ph/0512066
24. M. Czakon, U. Haisch, M. Misiak, JHEP **0703**, 008 (2007). hep-ph/0612329
25. W. Altmannshofer, P. Paradisi, D.M. Straub, JHEP **1204**, 008 (2012). arXiv:1111.1257 [hep-ph]
26. F. Beaujean, C. Bobeth, D. van Dyk, C. Wacker, JHEP **1208**, 030 (2012). arXiv:1205.1838 [hep-ph]
27. T. Hurth, F. Mahmoudi, Nucl. Phys. B **865**, 461 (2012). arXiv:1207.0688 [hep-ph]
28. S. Descotes-Genon, J. Matias, M. Ramon, J. Virto, JHEP **1301**, 048 (2013). arXiv:1207.2753 [hep-ph]
29. F. Kruger, L.M. Sehgal, N. Sinha, R. Sinha, Phys. Rev. D **61**, 114028 (2000). [Erratum-ibid. D **63** (2001) 019901]. hep-ph/9907386
30. A. Faessler, T. Gutsche, M.A. Ivanov, J.G. Korner, V.E. Lyubovitskij, Eur. Phys. J. direct C **4**, 18 (2002). hep-ph/0205287
31. A.K. Alok, A. Datta, A. Dighe, M. Duraisamy, D. Ghosh, D. London, JHEP **1111**, 121 (2011). arXiv:1008.2367 [hep-ph]
32. S. Jäger, J. Martin Camalich, JHEP **1305**, 043 (2013). arXiv:1212.2263 [hep-ph]
33. F. Kruger, J. Matias, Phys. Rev. D **71**, 094009 (2005). hep-ph/0502060
34. D. Becirevic, E. Schneider, Nucl. Phys. B **854**, 321 (2012). arXiv:1106.3283 [hep-ph]
35. J. Matias, F. Mescia, M. Ramon, J. Virto, JHEP **1204**, 104 (2012). arXiv:1202.4266 [hep-ph]
36. C. Bobeth, G. Hiller, D. van Dyk, JHEP **1007**, 098 (2010). arXiv:1006.5013 [hep-ph]
37. C. Bobeth, G. Hiller, D. van Dyk, Phys. Rev. D **87**, 034016 (2013). arXiv:1212.2321 [hep-ph]
38. S. Descotes-Genon, T. Hurth, J. Matias, J. Virto, JHEP **1305**, 137 (2013). arXiv:1303.5794 [hep-ph]
39. F. Mahmoudi, Comput. Phys. Commun. **178**, 745 (2008). arXiv:0710.2067 [hep-ph]
40. F. Mahmoudi, Comput. Phys. Commun. **180**, 1579 (2009). arXiv:0808.3144 [hep-ph]
41. A.J. Buras, F. De Fazio, J. Girrbach, JHEP **1302**, 116 (2013). arXiv:1211.1896 [hep-ph]
42. A.J. Buras, F. De Fazio, J. Girrbach. arXiv:1311.6729 [hep-ph]
43. A. Behring, C. Gross, G. Hiller, S. Schacht, JHEP **1208**, 152 (2012). arXiv:1205.1500 [hep-ph]
44. F. Mahmoudi, S. Neshatpour, J. Orloff, JHEP **1208**, 092 (2012). arXiv:1205.1845 [hep-ph]
45. B.C. Allanach, Comput. Phys. Commun. **143**, 305 (2002). hep-ph/0104145
46. M. Beneke, T. Feldmann, D. Seidel, Nucl. Phys. B **612**, 25 (2001). hep-ph/0106067
47. M. Beneke, T.Feldmann, D. Seidel. Eur. Phys. J. C **41**, 173 (2005). hep-ph/0412400
48. J. Charles, A. Le Yaouanc, L. Oliver, O. Pene, J.C. Raynal, Phys. Rev. D **60**, 014001 (1999). hep-ph/9812358
49. M. Beneke, T. Feldmann, Nucl. Phys. B **592**, 3 (2001). hep-ph/0008255
50. M. Beylich, G. Buchalla, T. Feldmann, Eur. Phys. J. C **71**, 1635 (2011). arXiv:1101.5118 [hep-ph]
51. B. Grinstein, D. Pirjol, Phys. Rev. D **70**, 114005 (2004). hep-ph/0404250
52. A. Khodjamirian, T. Mannel, A.A. Pivovarov, Y.-M. Wang, JHEP **1009**, 089 (2010). arXiv:1006.4945 [hep-ph]
53. D. Becirevic, V. Lubicz, F. Mescia, Nucl. Phys. B **769**, 31 (2007). hep-ph/0611295
54. A. Djouadi et al. [MSSM Working Group Collaboration]. hep-ph/9901246
55. A. Arbey, M. Battaglia, A. Djouadi, F. Mahmoudi, Phys. Lett. B **720**, 153 (2013). arXiv:1211.4004 [hep-ph]
56. Nicola Serra, private communication
57. [ATLAS Collaboration], ATLAS-CONF-2013-014
58. [CMS Collaboration], CMS-PAS-HIG-13-002
59. [ATLAS Collaboration], ATLAS-CONF-2013-047
60. P. Bechtle, T. Bringmann, K. Desch, H. Dreiner, M. Hamer, C. Hensel, M. Kramer, N. Nguyen et al., JHEP **1206**, 098 (2012). arXiv:1204.4199 [hep-ph]
61. C. Balazs, A. Buckley, D. Carter, B. Farmer, M. White, Eur. Phys. J. C **73**, 2563 (2013). arXiv:1205.1568 [hep-ph]
62. J.P. Lees et al., BaBar Collaboration. Phys. Rev. Lett. **109**, 101802 (2012). arXiv:1205.5442 [hep-ex]
63. J.P. Lees et al., BaBar Collaboration. Phys. Rev. D **88**, 072012 (2013). arXiv:1303.0571 [hep-ex]